scientific reports

Check for updates

OPEN

Morphological and environmental analysis of the glacier ice alga *Ancylonema alaskanum*

Marta J. Fiołka[1]✉, Weronika Sofińska-Chmiel[2], Lenka Procházková[3], Sylwia Mieszawska[4], Magdalena Dryglewska[5], Krzysztof Skrzypiec[2] & Jerzy Wydrych[6]

In the presented study, the cells of the glacial alga *Ancylonema alaskanum* collected in the Austrian Alps were analyzed. Algae were imaged both in their natural environment and in laboratory conditions using transmitted light and fluorescence microscopy. Using appropriate fluorochromes, the cell wall and cell organelles were studied. Oval nuclei located in the middle of the cell next to the chloroplasts and active mitochondria as well as lipid thylakoids of chloroplasts were imaged. Scanning electron microscopy showed that the surface of the algal cell wall was not significantly differentiated, and atomic force microscope imaging recorded little roughness. The SEM EDS analysis revealed that carbon, nitrogen, oxygen, and magnesium were the main components of the cells. It is worth emphasizing that the analyzed living algal cells were obtained directly from the glacier surface and demonstrated normal respiratory processes i.e. undisturbed physiological functions. Additionally, the mineral material accompanying the cells in their natural environment - fragments of the rock were imaged by Differential Interference Contrast microscopy and analyzed by Fourier Transform Infrared Spectroscopy. The study provides new data on the morphology and physicochemical characteristics of *A. alaskanum*, contributing to a more comprehensive characterization of their place in this harsh ecosystem.

Keywords Glacier ice algae, *Ancylonema alaskanum*, Staining organelles, Microscopy analysis, Spectroscopy analysis, Mineral material

The recent fast melting of glaciers and ice sheets is now considered a symbol of climate change. Many complex mechanisms are involved in ice melting[1]. Among these processes, surface darkening caused by organic material on the ice has recently gained attention from the scientific community. The process of melting glaciers is currently an important and frequently discussed topic in scientific journals, popular science literature, and Internet portals. Due to the existence of white surfaces, glaciers reflect up to 99% of solar radiation, thereby protecting the atmosphere from warming[2]. It is believed that even a small reduction in snow cover or snow albedo will have a huge impact on reducing the protective properties of the cryosphere, which will contribute to global warming[3–5]. Glacier surfaces are inhabited by diverse and dynamically interacting microbial communities[6–8]. The melting of glaciers is undoubtedly related to the presence of microorganisms on the ice surface, which lower its albedo and cause its melting[9]. Blooms can be caused by microorganisms and become visible only when the rate of their multiplication increases substantially so that their huge quantities suddenly appear in one place. As is widely known, white reflects considerable amounts of sunlight, while black absorbs it. Therefore, the darker the ice becomes, the faster it melts at the same level of exposure to solar energy[10]. As the ice melts at increasing rates, more abundant algae grow on its surface, as they are provided with the liquid water and air they need to survive. Algae multiply and the glacier surface turns darker. Anything that darkens the ice causes it to melt because it accelerates the absorption of radiation. Additionally, these microorganisms living in extreme conditions on the ice surface often combine with inorganic material in the form of mineral dust, creating dark sediment –

[1]Department of Immunobiology, Institute of Biological Sciences, Faculty of Biology and Biotechnology, Maria Curie-Skłodowska University, Lublin, Poland. [2]Analytical Laboratory, Institute of Chemistry, Maria Curie-Skłodowska University , Lublin, Poland. [3]Department of Ecology, Faculty of Science, Charles University, Prague, Czech Republic. [4]Chair and Department of Medical Microbiology, Medical University of Lublin, Lublin, Poland. [5]Department of Rheumatology and Connective Tissue Diseases, Medical University of Lublin, Lublin, Poland. [6]Department of Functional Anatomy and Cytobiology, Institute of Biological Sciences, Faculty of Biology and Biotechnology, Maria Curie-Skłodowska University, Lublin, Poland. ✉email: marta.fiolka@poczta.umcs.lublin.pl

cryoconite[11,12]. Scientists have evidenced that this process leads to increased absorption of visible radiation[13,14]. All this adds up to the final result of the melting ice, which is currently raising concern.

There are numerous studies on the biomass of algae on glacier surfaces[9], but only a few algal species contribute to the biomass[15]. On the other hand, algae represent a vast, still largely unexplored biomass that could potentially be used in industry or medicine. In order to survive in extremely harsh environmental conditions, algae have developed unique adaptive mechanisms. Their adaptive abilities in response to extreme conditions – such as very low temperatures, high levels of UV radiation, and changes in nutrient availability – result in the production of substances with high therapeutic potential. These include, among others, dyes and polyunsaturated fatty acids with anti-inflammatory and immunomodulatory effects[16,17]. Studies on the mechanisms protecting cells from damage caused by low temperatures may help develop new therapies, as is the case with marine algae[18].

The functioning of glacial ecosystems is dependent on the presence of microorganisms[8]. Glacier ice algae are extraordinary organisms that exhibit some of the most extreme adaptations to low temperatures and low light ever observed in nature. This unique feature allows these algae to quickly produce biomass in spring when light conditions improve. *Ancylonema alaskanum* (formerly *Mesotaenium berggrenii* var. *alaskanum*) is a microorganism that was found in an Austrian Alps glacier[19,20]. These microscopic single-celled algae growing in one of the most extreme habitats on Earth - glaciers also influence their modeling. This species was also observed in cold regions of the world, such as Greenland[21,22], southern Chile[23], and Svalbard[20]. Blooms of streptophytic algae living on glacier surfaces are formed by actively dividing vegetative cells. The reports about their zygospores are only scarce[24], unlike snow algae, whose cysts cause snow to turn red[17,20]. The relatively sparse information about this single-celled alga prompted us to analyze its cells and characterize it morphologically and environmentally. These algae stop dividing when isolated from the natural environment due to the difficulty of simulating natural environmental conditions[25–27].

The aim of the research was to analyze living algal cells originating from the natural environment using biological and chemical methods. The use of various techniques ensured a better insight into these cells in survival conditions. Details of their cellular structure can help us understand how these cells cope with the exposed glacier ice surface. The approach to the analysis of algal cells on which there is little data was possible thanks to the conducted interdisciplinary research - a combination of microscopic analyses from the field of microbiology with chemical analyses from the field of spectroscopic sciences. This research was supported by the knowledge of an experienced phycologist who also collected these samples from the glacier. The joint effort of specialists from various fields creates a new approach to the subject and provides a broader characterization of organisms, such as the *A. alaskanum* alga species.

Materials and methods

Sample collection

Samples containing living glacier ice algae *Ancylonema alaskanum* were collected on 22 August, 2022 in the Austrian Alps (Langtaler Ferner, Sölden, Tirol) at N46° 47.594' E11° 00.941', altitude 2634 m, sample code WP314 (Fig. 1). The harvested glacier ice was gently melted in the dark at 4 °C overnight. Glacier meltwater pH was 5.7 and electric conductivity was 4.8 $\mu S.cm^{-1}$. Larger debris was removed by sieving the meltwater through an 800, 400, 200, and 140 µm mesh size stainless steel sieve tower (Retsch, Germany). Until further processing, the cells were kept in original glacier meltwater in an illuminated 5 °C incubator for a few weeks.

Brightfield light microscopy

The algal cells were observed and imaged using a Zeiss Axiovert 220 M with a scanning head LSM 5 Pa confocal microscope. The cells were placed on a glass slide in an amount of 2 µl of glacier meltwater, covered with a coverslip, and imaged using oil immersion at 100x magnification. The rock material was observed using the differential interference contrast (DIC) technique with a Nikon Eclipse MA200 (Japan) microscope under 60x magnification.

Fluorescence microscopy

The Calcofluor white dye is mainly used to stain fungal cell walls because it binds to chitin, causing blue fluorescence of the cell contours[28–30]. This fluorochrome also binds to cellulose, which is a component of the cell wall of algae and vascular plants[31–33]. Calcofluor white (Fluka) was added to the aqueous suspension of algal cells in a 1:2 ratio and incubated for 10 min in complete darkness. The algal cells were imaged with a confocal microscope as described above. The excitation wavelength for Calcofluor white was $\lambda = 365$ nm, emission $\lambda = 475$ nm, and fluorescence color – blue. The cells were imaged with a Zeiss LSM 5 Pa fluorescence microscope at 100× magnification.

A mixture of fluorescent dyes: Hoechst 33342 (Sigma) and propidium iodide (Sigma) was used to visualize algal cell nuclei[29,34]. The staining mixture was added in a 1:1 volume to the algal cell suspension and then incubated for 5 min at 37 °C in the dark. The algal cells were analyzed using a Zeiss LSM 5 Pa fluorescence microscope. Normal cell nuclei stain intensely blue. The nuclei of apoptotic cells are fragmented and emit intensely blue fluorescence, and necrotic cells are characterized by pink nuclei. The excitation wavelength for Hoechst 33342 and propidium iodide was $\lambda = 365$ nm, emission $\lambda = 454$ nm for Hoechst 33342, and emission $\lambda = 417$ nm for propidium iodide. The samples were observed with a Zeiss LSM 5 Pa fluorescence microscope at 100× magnification.

The Rhodamine 123 dye (ThermoFisher Scientific) is commonly used to stain the membranes of properly functioning mitochondria[35]. Active mitochondria emit green fluorescence. Cells with impaired mitochondrial function have no membrane potential and do not emit any fluorescence. Rhodamine 123 was used at a concentration of 120 $\mu g\ mL^{-1}$. The negative control was performed using sodium azide, which is an inhibitor of the mitochondrial respiration pathway[36]. A 1.3% solution of sodium azide (Sigma) was incubated with the algal

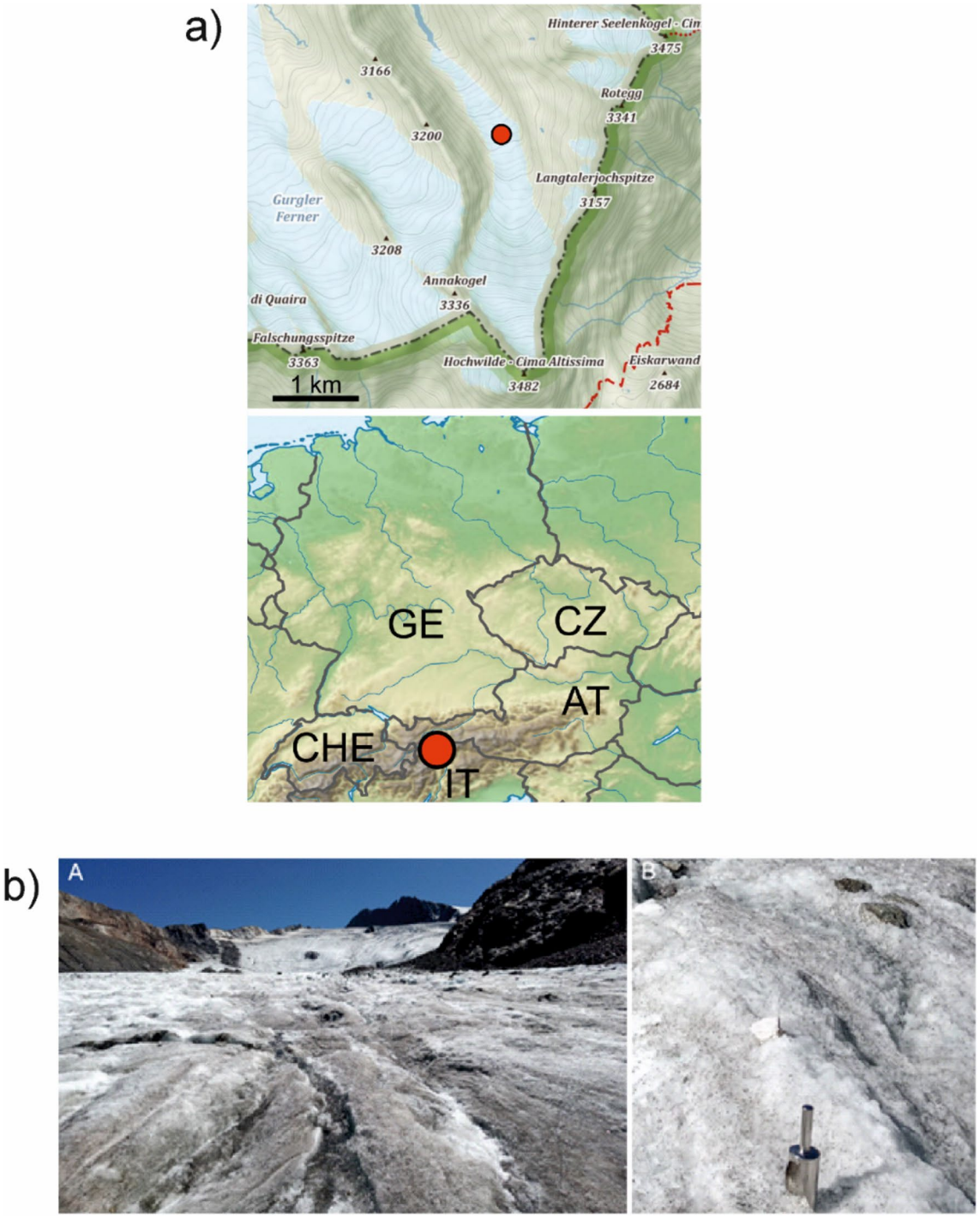

Fig. 1. (**a**) Overview of the sampling sites of *Ancylonema alaskanum*: (**b**) (**A**) Sampling location at Langtaler Ferner, a glacier in Sölden, Tyrol, Austria (23 Aug 2022, field sample WP314). (**B**) Detailed view of the faintly brownish glacier ice surface before harvest.

cells in a 1:1 ratio for 10 min at room temperature. Controls were incubated with Rhodamine 123 at 37 °C for 20 min and then washed 3 times with sterile water. Samples were transferred to microscope slides and imaged with a Zeiss LSM 5 Pa fluorescence microscope at 100× magnification[37]. The excitation wavelength for Rhodamine 123 was $\lambda = 470$ nm and emission $\lambda = 528$ nm; dyed structure – the membrane of active mitochondria.

The fluorescent dye Nile Red (Sigma-Aldrich) was used to determine lipids in the *A. alaskanum* algal cells[38]. Nile Red (NR, 9-diethylamino-5 H-benzo[α]phenoxazine-5-one) is one of the most commonly used fluorescent dyes. It is lipophilic in nature, i.e. it is able to bind to intracellular neutral lipids[39] with a linear correlation between NR fluorescence and neutral lipid content[40]. A 1:10 DMSO: PBS (pH 7.2) solution was used for staining. The algal suspension was mixed in a 1:1 ratio with the prepared dye solution and incubated for 10 min in the

dark at room temperature; then, it was placed on a microscope slide and observed using immersion at 100× magnification with a Zeiss LSM 5 Pa fluorescence microscope at excitation wavelength λ = 546 nm and emission λ = 635 nm.

Acridine orange is a fluorochrome used to stain living and fixed microbial cells[41]. This fluorescent dye binds nucleic acids. It has the ability to penetrate cells and emit green fluorescence when bound to dsDNA and red fluorescence when bound to ssDNA or RNA. This fluorochrome is permeable to cells and interacts with DNA and RNA through intercalation or electrostatic attraction, respectively. Acridine orange can be used to stain acidic organelles, such as lysosomes, autosomes, or vacuoles[42]. It emits orange fluorescence inside the organelle at low pH. The *A. alaskanum* cell suspension was mixed with a 0.001% aqueous acridine orange solution in a 1:1 volume ratio and incubated in the dark for 10 min. The cells were observed at the excitation wavelength λ = 470 nm and emission λ = 520 nm[43] using a Zeiss LSM 5 Pa fluorescence microscope at 100× magnification[44].

Scanning electron microscopy (SEM)

The algal cells were visualized using the SEM technique. The cells together with the rock material were centrifuged and the supernatant was suspended in a fixative (10 ml 0.1 M phosphate buffer pH = 7.0, 10 ml 8% glutaraldehyde, 200 mg sucrose) and then incubated for 4–6 h at room temperature. Then, 1.5% OsO_4 was added to the pellet and centrifuged for 30 min at 2500 g. Next, OsO_4 was removed and the cells were suspended in 0.1 M phosphate buffer, followed by centrifugation for 30 min at 2500 g. The algal cells were dehydrated in acetone solutions with increasing concentrations: at 30%, 50%, 70%, and twice at 100%. The cells were transferred to SEM trays and dried in a silica gel desiccator for 24 h. The samples were sputtered with gold using a K550X sputter coater (Quorum Technologies). The algal cells were imaged with a Vega 3 scanning electron microscope (Tescan, Czech Republic)[41,44].

Atomic force microscopy (AFM) analysis of *Ancylonema alaskanum* cells

Samples for the AFM analysis were prepared exactly as for scanning electron microscopy. The preparations were not sputtered with gold, but were applied to mica disks, dried in a silica gel desiccator for 24 h, and then analyzed using an atomic force microscope. The surface of the *A. alaskanum* cells was measured using NanoScope V AFM (atomic force microscope) in the Peak-Force Quantitative Nanomechanical Mapping Mode (Bruker, Veeco Instruments Inc., Billerica, MA, USA) and NanoScope 8.15 software. The nominal spring constant of the RTESPA probe (Bruker, Billerica, MA, USA) (silicone tip on the nitride lever) was 40 N/m[43]. The resolution of the scans obtained was 256 × 256 pixels. The scan rate was 0.5 Hz. Height and Peak Force Error images were obtained simultaneously. The data were analyzed with Nanoscope Analysis ver. 1.40 software (VEECO, USA).

SEM/EDS analysis

Microscopic examinations of algal samples were performed using a high-resolution scanning electron-ion microscope Quanta 3D FEG (FEI). Microscopic images of the sample surface topography were taken in high vacuum (HV), in a topographic contrast mode, SE. Before performing SEM analyses, the tested samples were sputtered with a Pd/Au layer using a Polaron SC7640 sputter coater. Images of the samples were recorded at a magnification of x 10 000. Microanalysis (elemental composition) of the tested samples was also performed using EDS X-ray spectrometry. The FEI Quanta 3D FEG microscope is equipped with an EDS X-ray spectrometer with a fast Octane Elect Plus detector, which allows precise analysis of the elemental composition, including mapping of the distribution of elements[44].

FTIR spectroscopy

Infrared spectroscopy is an analytical technique that uses the interaction of IR radiation with tested biological or chemical samples[45,46]. Part of the radiation is specifically absorbed by the analyzed samples. Absorption of electromagnetic radiation in the infrared range causes changes in the vibrational energy and rotational energy of the molecule. The radiation passing through the studied sample is recorded. Since different molecules with different structures are characterized by different spectra, these spectra can be used to identify and observe subtle differences in the molecules[47,48]. FTIR spectroscopy was used to identify minerals accompanying the algal samples. The samples were air-dried and subjected to FTIR analysis. Due to the very small size of the objects studied, a Nicolet iN10 MX FTIR microscope (Thermo Scientific) was used. The studies were performed using the reflectance technique with a detector cooled by liquid nitrogen. The MCTA detector guarantees signal stability in the mid-infrared spectrum: 4000–650 cm^{-1}. For each spectrum, 256 scans were performed with a resolution of 8 cm^{-1}.

Results

Imaging of algal cells using Brightfield light microscopy

The *Ancylonema alaskanum* algal cells appeared in the brightfield light microscope images as cylindrical structures with broadly rounded edges and visible grains inside the cells (Fig. 2). The cells were measured, and their cell size distribution is shown in Fig. 3.

The largest group of cells, in percentage terms as much as 29.7%, were cells with dimensions of 10–12 µm, marked in green in the histogram (Fig. 3) with a mean cell size of 11.0 µm. Cells sized 12–14 µm were also present in a significant number, i.e. 25%, as reflected in the yellow part of the histogram, with a mean cell size of 12.8 µm. Cells larger than 14–16 µm accounted for nearly 20% of the entire population (marked in blue on the chart). Cells with a size of 16–18 µm accounted for 5.7% and are marked in gray in the graph (mean cell size 16.7 µm). The largest cells, 16–18 µm and over 18 µm, represented the lowest percentage, i.e. 1.63% and 0.81%, respectively (blue and red in the graph) (Fig. 3).

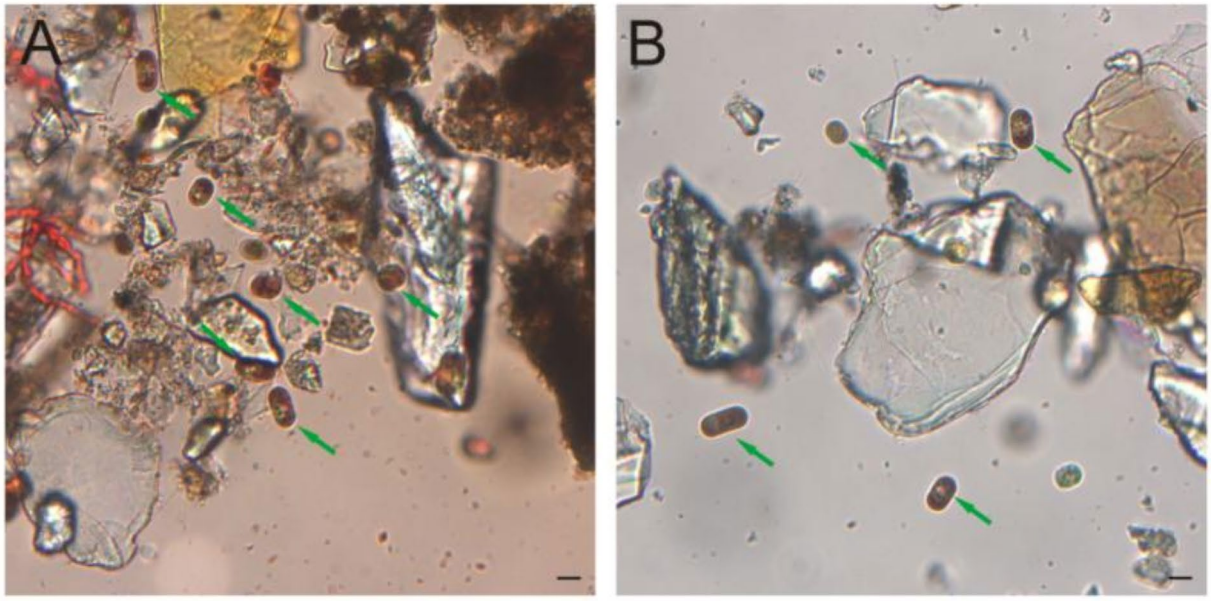

Fig. 2. (**A**, **B**). *Ancylonema alaskanum* algal cells observed under a transmitted light microscope (pointed by green arrows). Scale bar corresponds to 10 µm.

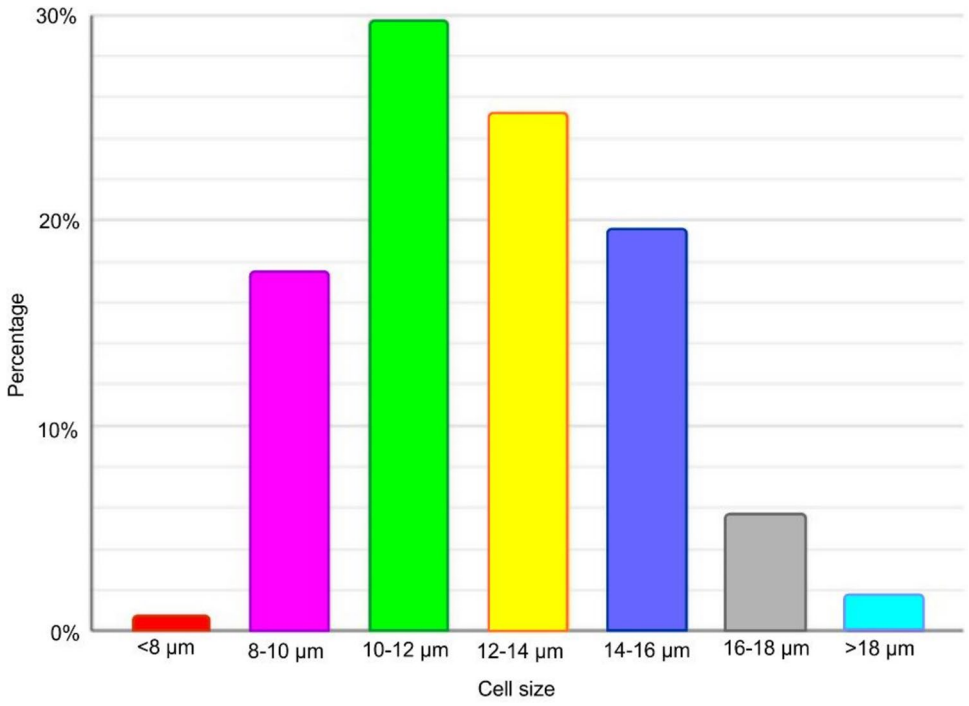

Cell size	<8 µm	8-10 µm	10-12 µm	12-14 µm	14-16 µm	16-18 µm	>18 µm
Number of cells	4	86	146	124	96	28	8
Mean size	7.6	9.2	10.9	12.7	14.87	16.8	18.6
Std dev.	0.01	0.49	0.62	0.49	0.58	0.48	0.53

Fig. 3. Size of algal cells in the collected samples. Sets of cells of a specific size are marked with colors.

Staining of cell structures using fluorescence microscopy

The cell wall was stained with the Calcofluor white fluorochrome. The images in Fig. 4A1,A2,A3,A4 showed cell wall staining. It is seen as blue fluorescence at the periphery of the cell, where A1 and A3 are stained control images in transmitted light.

After staining the algal cells with a mixture of Hoechst 33,342 and propidium iodide dyes, the cell nuclei turned blue (Fig. 4B1,B3 – stained cells in transmitted light; Fig. 4B2,B4 - stained cell with emitted fluorescence). They were visible as compact and round structures in the central part of the cell, near the chloroplasts emitting red fluorescence in these conditions (Fig. 4B2,B4). The cells in transmitted light are shown in micrographs B1 and B3. Staining the nuclei with the mixture of fluorochromes showed that the cells were neither necrotic nor apoptotic. The cells appeared to be alive and functioning properly.

The Rhodamine 123 stained active mitochondria, which fluoresced in green. The structures were visible as elongated structures located in the central part of the cell (Fig. 4C1,C3 - control, Fig. 4C2,C4 - stained cell). The fluorescent signal from the mitochondria came from a very limited central area in the cells. The cytoplasm was highly compressed, as most of the cell volume was occupied by large vacuoles (typical of Streptophytes).

The Nile red fluorochrome was used to locate lipids in the algal cells. They were visible as double oval red fluorescent structures occupying half of the cell lumen (Fig. 4D1 - control, D2 - stained cell, D3 - control, D4 - stained cell).

In addition, the acidic cell compartments were stained with acridine orange, which caused to the compartments to fluoresce red (Fig. 5A1,B1,C1,D1 – stained cells observed with transmitted light, Fig. 5A2,B2,C2,D2 - stained cells under a specific type of filter for fluorescence observation). The green areas of the cell visible in transmitted light gave a red fluorescent signal after using the dye for both fat and acidic compartments. In the case of fat

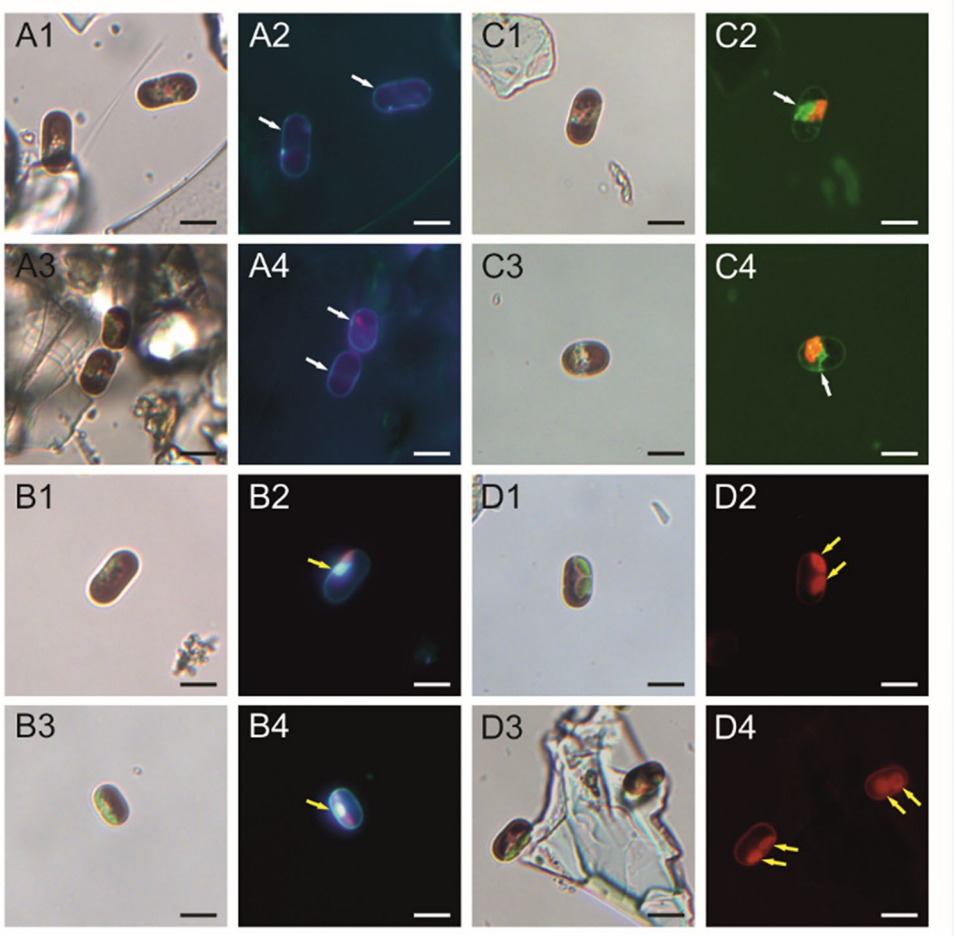

Fig. 4. *Ancylonema alaskanum* algal cells after staining of the cell wall, organelles, and fats with fluorochromes: **A1**, **A2**, **A3**, **A4**—Calcofluor white—cell wall staining (**A1**, **A3** – cells observed with transmitted light, **A2**, **A4** – stained cells with emitted fluorescence); **B1**, **B2**, **B3**, **B4**—a mixture of Hoechst 33,342 and propidium iodide—nucleus staining (**B1**, **B3** – cells observed with transmitted light, **B2**, **B4** – stained cells with emitted fluorescence); **C1**, **C2**, **C3**, **C4**,—Rhodamine 123—mitochondria staining (**C1**, **C3** – cells observed with transmitted light **C2**, **C4** – stained cells with emitted fluorescence); **D1**, **D2**, **D3**, **D4**—Nile red – lipid staining (**D1**, **D3** – cells observed with transmitted light, **D2**, **D4** – stained cells with emitted fluorescence). The scale bar corresponds to 10 μm.

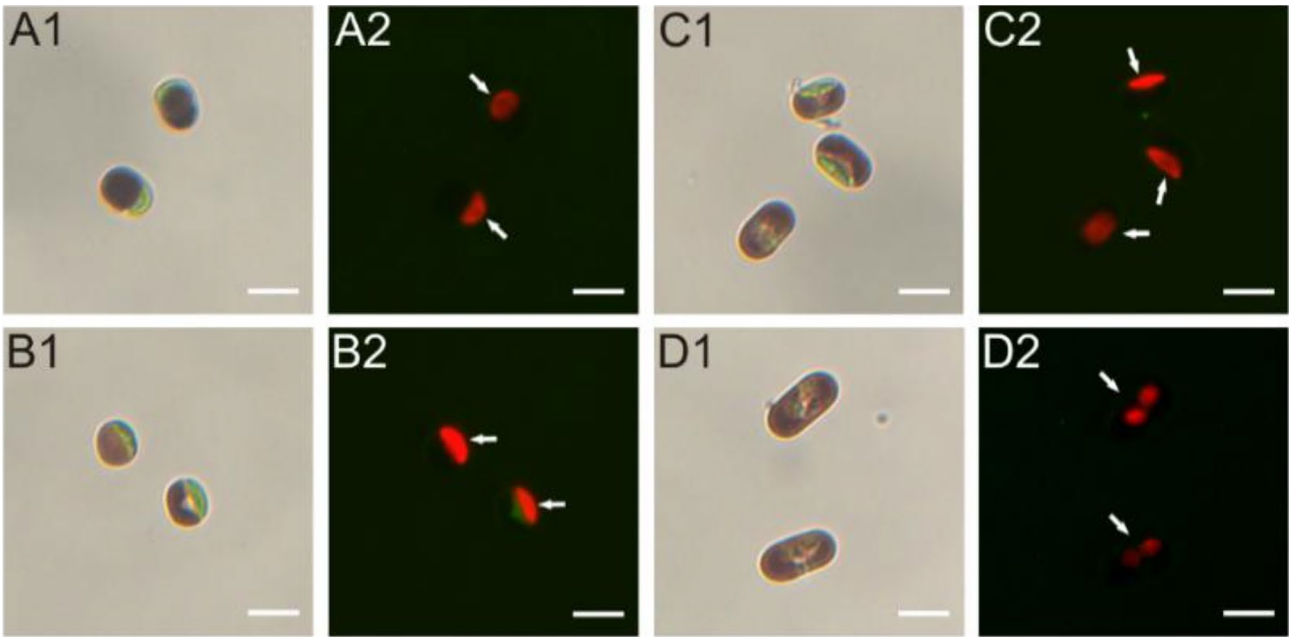

Fig. 5. *Ancylonema alaskanum* algal cells after staining of acidic compartments with acridine orange (A1-D2); left panels for every staining variant show cells observed with transmitted light; right panels - stained cells with emitted fluorescence. The scale bar corresponds to 10 µm.

staining, a red outline of the cell was visible, which was not observed after staining acidic structures with acridine orange.

SEM imaging of algal cells

The cell imaging using scanning electron microscopy visualized the morphology and surface of the algal cell wall (Fig. 4). The surface of the cell wall analyzed using this technique is rather flattened and without any sculpture. The cells are oval with rounded edges, and single grains are visible on the wall surface. The oval shape of the cells causes the edges of the algal cells visible in the scanning electron microscope as brighter rims, which makes it possible to distinguish these structures from rock fragments.

Atomic force microscopy (AFM) imaging of algal cells

The surface of the algal cells was additionally imaged using atomic force microscopy, which gave information on the properties of the cell wall. The wall surface of two randomly selected cells was analyzed. The elevation profile of both analyzed areas was very similar. The roughness values were measured over the entire cell surface on 1000 nm x 1000 nm areas. The average surface (Ra) roughness and surface root-mean-square (RMS) roughness of the cells was: A1 - Ra = 9.05 nm, Rq = 11.4 nm. A2 - Ra = 8.84 nm, Rq = 11.6 nm. It can be seen that the surface of the walls varies to some extent. It is clearly slightly corrugated, and the visible reduction in the profile is a result of the natural oval shape of the cell. The many small peaks visible in the graphs indicate roughness of the cell surface (Fig. 5), which could not be seen in the SEM analysis.

SEM/EDS analysis

The SEM EDS studies showed that carbon, nitrogen, oxygen, and magnesium were the main elements in the composition of the *A. alaskanum* glacier ice algae. In addition, the presence of silicon, potassium, calcium, and iron was found in concentrations below 1% by mass. The SEM EDS test results are presented in Fig. 6.

Microscopic analysis of the rock material

The rock masses accompanying the algal cells were analyzed microscopically using the DIC function. The rock material looked in a characteristic way, showing coloration similar to that of a precious opal, which opalizes in a rainbow manner, shimmering with many colors (Fig. 7). The minerals had sharp, irregular edges and visible overlapping layers of rock material with a pearly lustre.

FTIR analysis of the rock material

The FTIR studies of the rock material accompanying the glacier ice algae showed the best match of the obtained spectrum to Nontronite from the HR Inorganic database, a mineral from the clay mineral group with the chemical formula $(CaO_{0.5},Na)_{0.3}Fe^{3+}2(Si, Al)_4O_{10}(OH)_2{\cdot}nH_2O$. The match coefficient of the obtained spectrum to the Nontronite spectrum from the database was HQI = 90.44. The differences in the spectra in the range of 3700 –3000 cm^{-1} and 1700–1500 cm^{-1} were caused by different water contents in the compared samples. In the

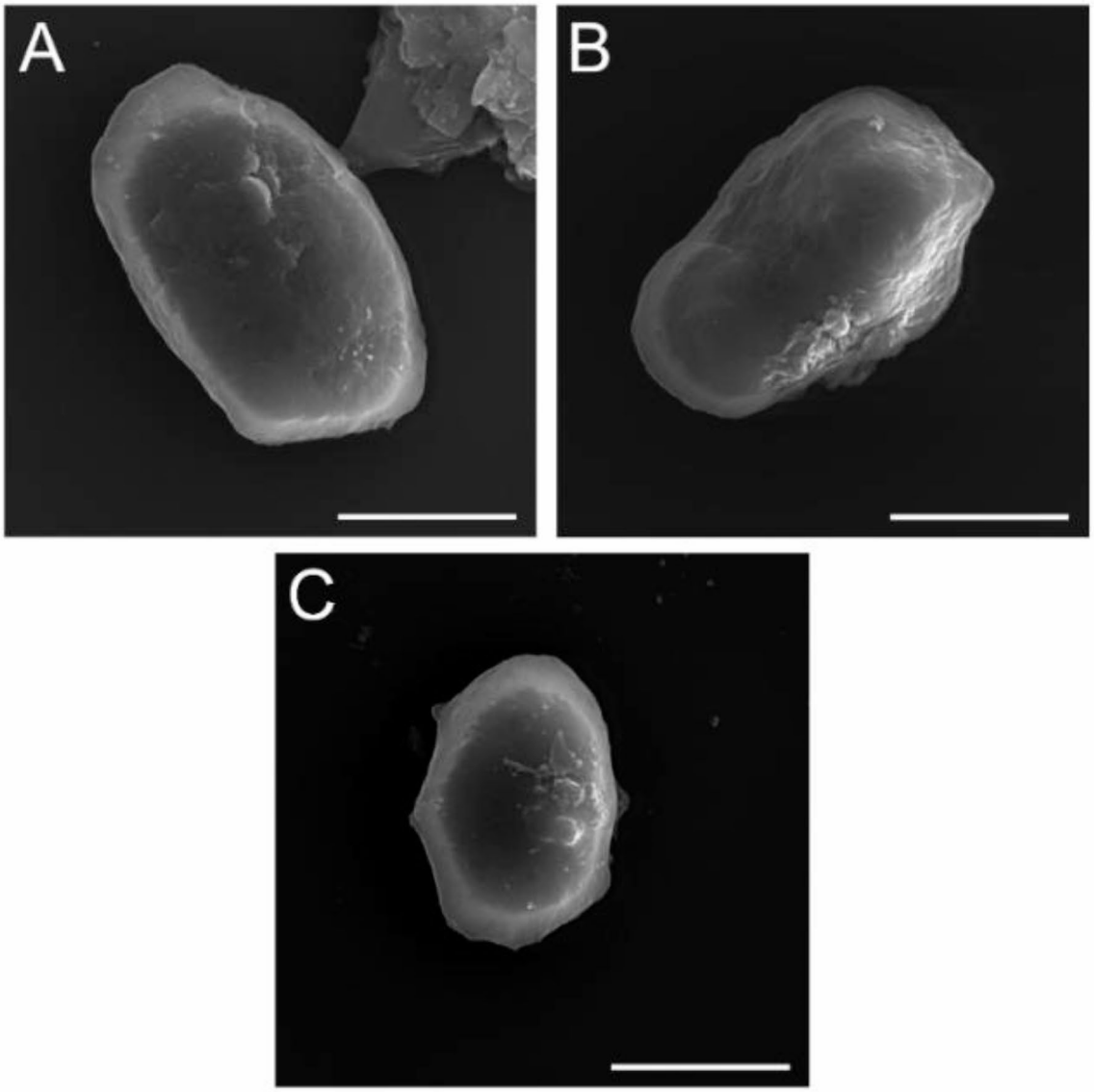

Fig. 6. *Ancylonema alaskanum* cells imaged by SEM (**A**, **B**, **C**). The scale bar corresponds to 10 µm.

Nontronite spectrum, much more intense bands characteristic of stretching vibrations of the -OH groups were observed.

The FTIR studies also facilitated the identification of another mineral accompanying the glacier algae. The obtained FTIR spectrum was subjected to a spectral search process using commercial databases. The best match was obtained to the illite spectrum from the HR Inorganic database. Illite is a mineral from the silicate group, classified as a clay mineral with the chemical formula $K_{0.6-0.85}Al_2(Si, Al)_4O_{10}(OH)_2$. The match coefficient of the obtained spectrum to the illite spectrum from the HR Inorganic database was HQI = 94.09 (Fig. 8).

Discussion

Due to the limited data available on the glacier ice alga *Ancylonema alaskanum*, it seemed appropriate to examine the morphology and structure of living cells collected in the field. The research carried out so far allows the comparison of two species of glacier ice algae. Another glacier ice alga *Ancylonema nordenskiöldii* found in Svalbard was previously analyzed by us using fluorescence microscopy, scanning electron microscopy, and atomic force microscopy techniques[44].

Calcofluor white was used to stain the algal cell wall. The fluorescent blue dye binds to the 1–3 beta and 1–4 beta polysaccharides of chitin, cellulose, and callose[49], which are present in the cell walls of fungi, plants, and algae. This fluorochrome is widely used in cell biology studies to stain the cell walls of both algae and land plants[33,50]. The comparison of *A. alaskanum* and *A. nordenskiöldii* cells indicated some similarities in their

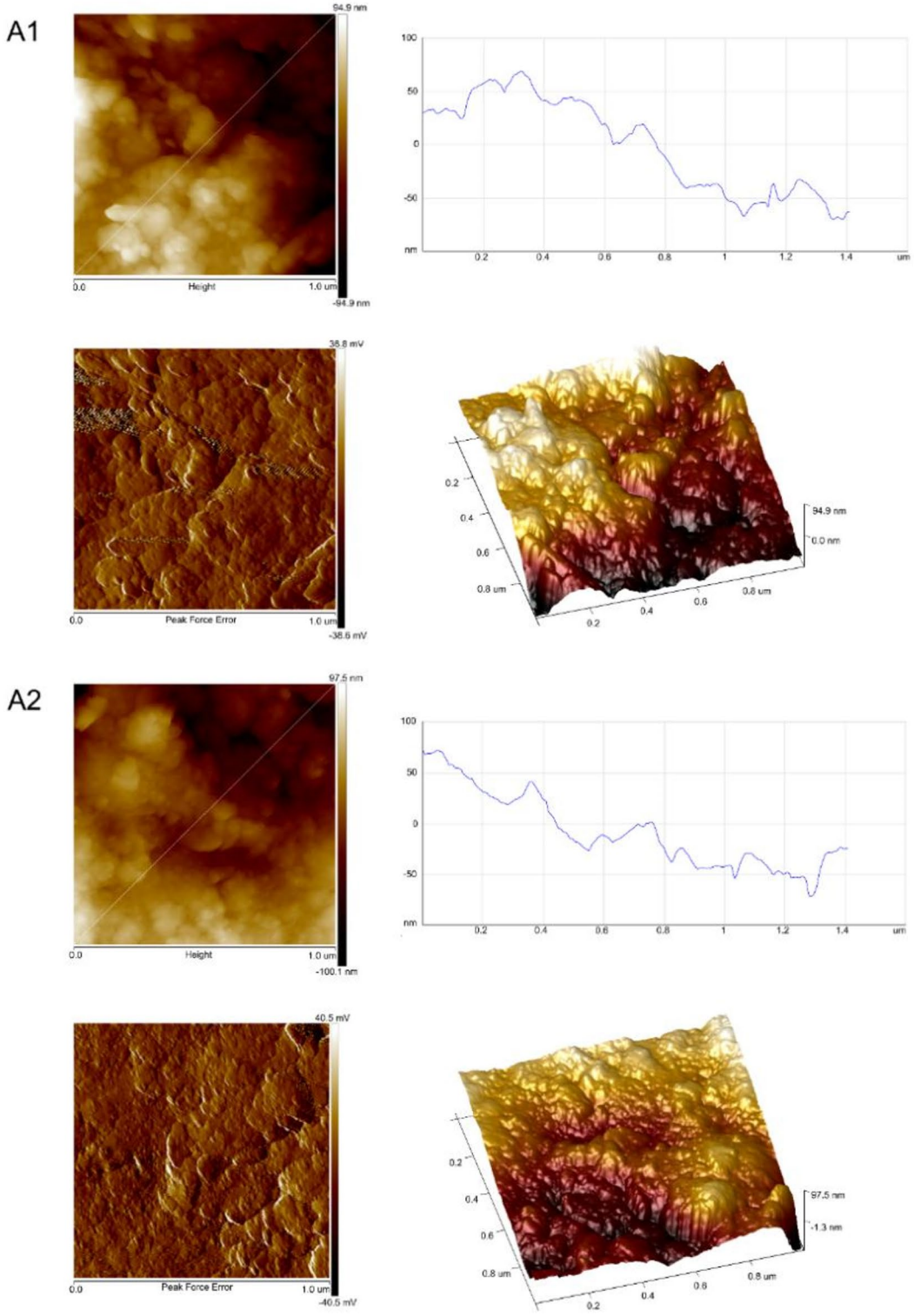

Fig. 7. *A. alaskanum* cell wall surface observed with AFM. A1, A2 1- surface of cells (left panel) and the height profile of cells (on right panel).

morphology; in both cases, the cell wall staining using Calcofluor white suggested its cellulose structure (Fig. 9). It is worth noting that *A. alaskanum* cells were not infected with a fungus, unlike the previously described *A. nordenskiöldii* from Svalbard[44], where chytrid-like fungi penetrating the latter species were noticed. In the analysis of the *A. alaskanum* cells, not a single cell attacked by the fungal parasite was observed, as revealed by fluorescent microscopy using Calcofluor white, which binds to the chitin of the fungal walls.

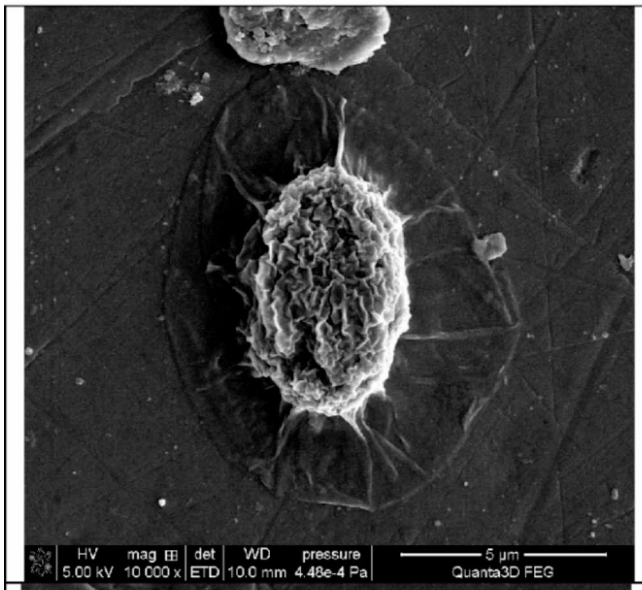

Element	% Mass concentration	% Atom concentration
C	56.31	64.94
N	12.16	12.02
O	18.27	15.82
Na	0.86	0.52
Mg	10.89	6.21
Si	0.21	0.10
K	0.26	0.09
Ca	0.37	0.13
Fe	0.66	0.16
Total	100.000	100.000

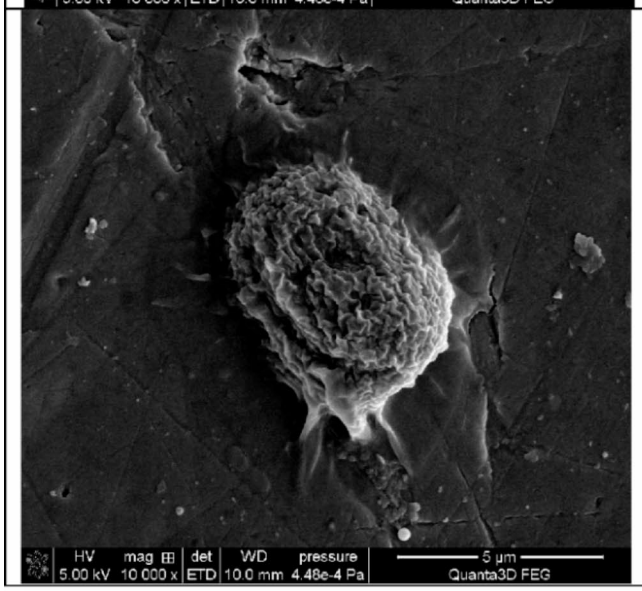

Element	% Mass concentration	% Atom concentration
C	57.77	65.91
N	13.42	13.13
O	17.46	14.95
Na	0.83	0.50
Mg	8.82	4.97
Si	0.25	0.12
K	0.26	0.09
Ca	0.31	0.11
Fe	0.87	0.21
Total	100.000	100.000

Fig. 8. SEM images of the *A. alaskanum* glacier ice algae and the elemental composition determined from these areas by the scanning electron microscopy with the EDS detector.

Mucous material production is a strategy for desiccation tolerance in many terrestrial Zygnematophyceae[51]. Remias and collaborators[25] reported a "fibrous layer" of the cell wall of *Ancylonema alaskanum* in a TEM picture, but such a possible extracellular matrix was not further discussed in the cited paper. Generally, arabinogalactan-proteins (highly glycosylated proteins) may be crucial for adhesion of cells to the substrate in Zygnematophyceae[52]. In the case of *Ancylonema alaskanum*, a very typical behavior of field cells in glacier meltwater was observed: little rock debris were surrounded by cells resembling "a raft with passengers". The mechanism remains to be elucidated to determine e.g. whether some cell wall compounds play a role in this phenomenon or whether this is rather a consequence of electrostatic gentle sticking to the quartz-like particle.

The SEM images showed that the cells were oval with small granules on the surface (Fig. 4). The observations carried out using a scanning electron microscope showed that the wall of *A. alaskanum* was definitely more stable than that of *A. nordenskiöldii*, as it was not as sensitive to dehydration as the very thin and delicate wall of *A. nordenskiöldii*[44]. The *A. alaskanum* cells fully retained their natural shape. In our studies, AFM analysis was used to characterize the cell wall surface and showed the diversity of this surface. The analyses of *A. alaskanum* revealed that the cell surface was not smooth but slightly ridged. After the AFM analysis, the surface topography was clearly visible (Fig. 5). The *A. alaskanum* cell wall surface is rougher than that of *A. nordenskiöldii*. The height profile determined by the atomic force microscope was characterized by many peaks, which was not observed in the profile of *A. nordenskiöldii* cells. In a study conducted by Permann and co-workers, AFM was recently used

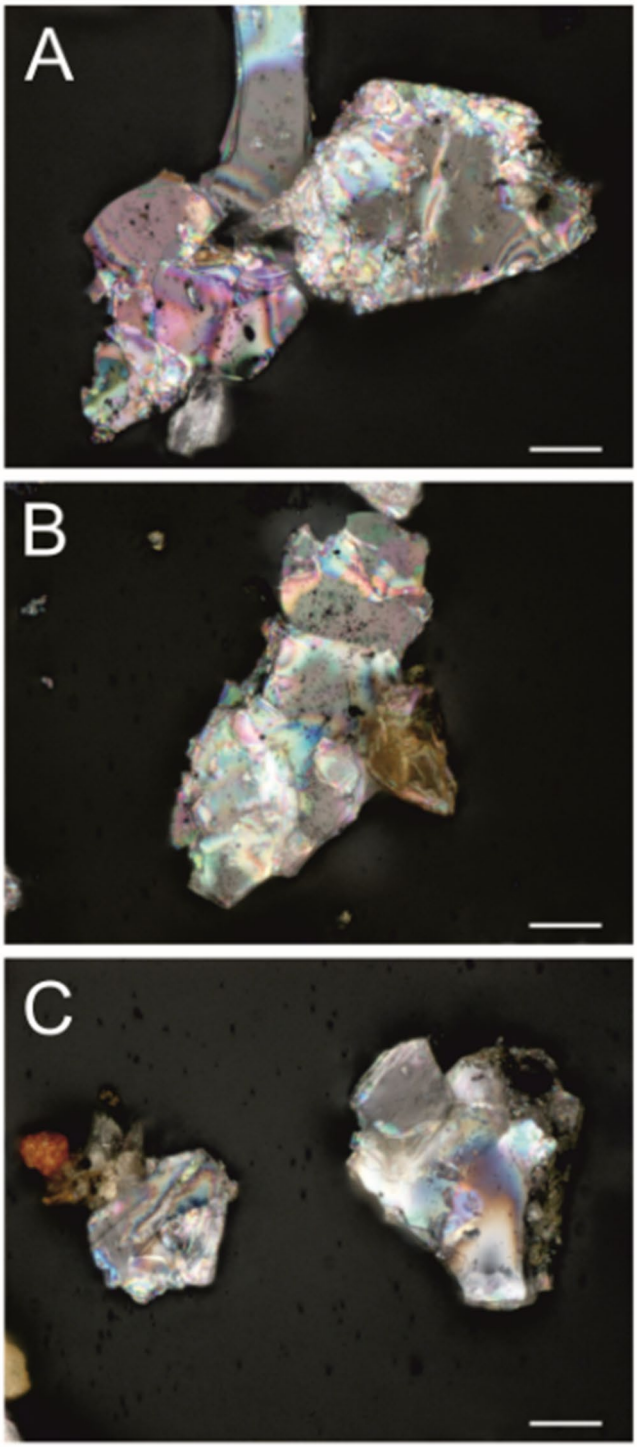

Fig. 9. (**A**, **B**, **C**). Fragments of shimmering with different colors rocks from *A. alaskanum* algal samples observed with DIC microscopy. The scale bar corresponds to 20 µm.

on high pressure freeze/freeze substitution fixed material of the cell walls of Zygnematophycean zygospores, which allowed the determination cell wall characteristics, such as adhesion and stifftness[53].

The analysis of cellular structures using fluorochromes dedicated for individual organelles revealed the distribution of these structures in the cell, indicating that the cells functioned properly without signs of apoptosis and necrosis. Hoechst 33,342 is a dye applied for the analysis of cell nuclei. It belongs to the group of blue fluorescent dyes used to stain DNA[54–56]. The visualized nucleus of *A. alaskanum* is located in the center of the

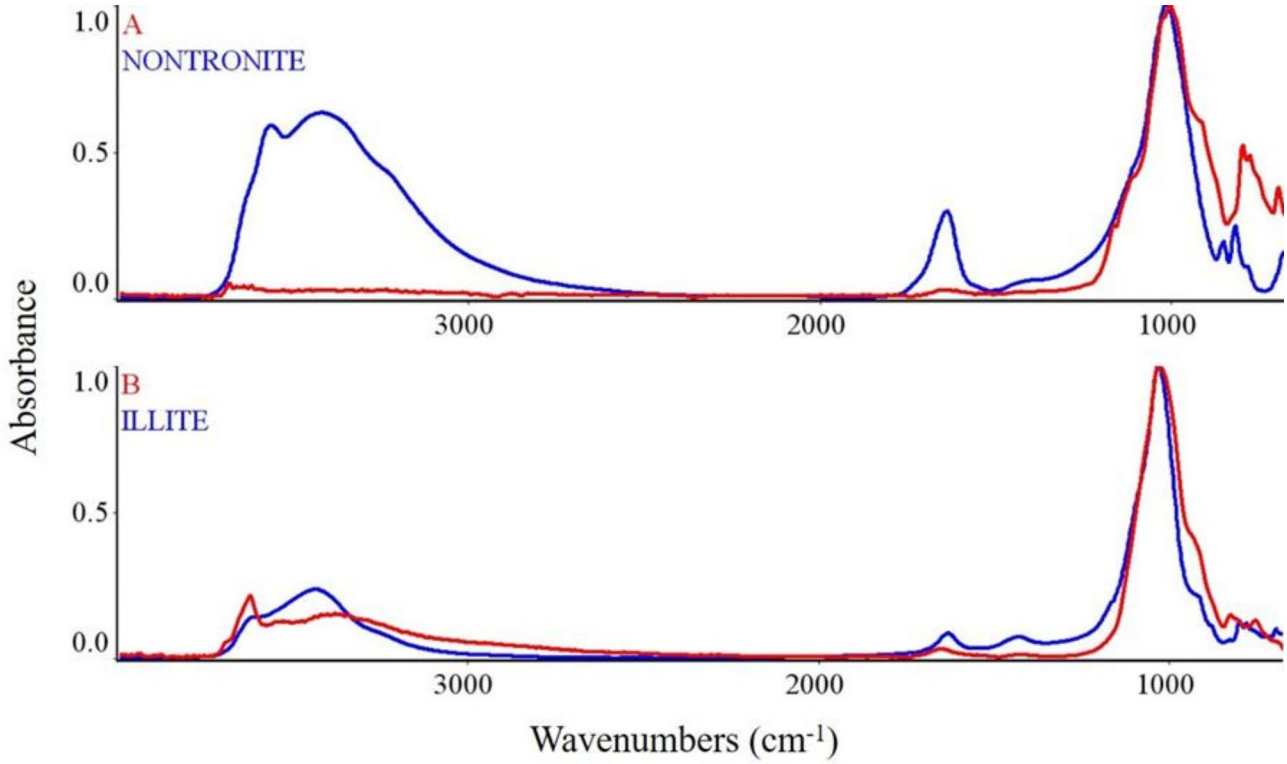

Fig. 10. Comparison of the FTIR spectra of samples A and B with the database.

cells and thus next to the parietal partly lobed chloroplasts; similar central location of the nucleus was reported for *A. nordenskiöldii*. After using a mixture of Hoechst 33,342 and propidium iodide, the nuclei of cells fluoresced blue and were compact. In the case of necrosis, the nuclei stain red, and in apoptosis they fluoresce white and blue and are clearly fragmented[29,37]. Such phenomena have not been observed in the cells studied (Fig. 9).

Mitochondrial imaging using fluorescent methods is an essential tool for studying the function of these cellular organelles[35]. Rhodamine 123 is a cationic fluorescent dye that is used in microscopy to specifically label respiring mitochondria. This fluorochrome distributes itself according to the negative membrane potential across the inner mitochondrial membrane, and loss of potential will result in loss of dye and therefore fluorescence intensity[57]. The dye has been used to monitor mitochondrial function in living algal cells. Brightly fluorescing active mitochondria are evidence of cell viability. Active mitochondria fluoresce green, while inactive ones do not fluoresce at all[37]. In the observed case, the process of the respiration process is not disturbed (Fig. 9).

Acidic cellular compartments stained with fluorochrome acridine orange correspond to the location of chloroplasts, which is consistent with the images of *A. alaskanum* presented in another article[20]. The chloroplast was recognized as an acidic compartment (Fig. 10), as this signal comes most likely from the lumen, which is acidic due to biochemical processes (i.e. proton accumulation in the lumen during the light part of photosynthesis and function of ATP synthase)[58–60].

Lipids are an integral part of the thylakoid membranes in chloroplasts as well as cytoplasmic membranes. Lipids of the thylakoid membranes of chloroplasts were bound and stained with fluorochromes dedicated to detecting lipids (Fig. 9). The comparison of the size of cells of *A. alaskanum* and *A. nordenskiöldii* showed that the former algae are almost half as long as the previously described glacier ice alga *A. nordenskiöldii*[44]. Although both *Ancylonema* species originate from glacier surface habitats, the differences in these cells are very significant.

An important conclusion is the confirmation of the suitability of the methods used to study glacier ice algal cells. Scanning microscopy and atomic force microscopy are very effective in characterizing cell morphology and analyzing cell wall topography. Fluorescence microscopy methods using appropriate fluorochromes distinguish cell organelles well and facilitate confirmation of physiological regularities.

Due to the accessibility of the bedrock, sampling the subglacial microbiome is much more difficult than from the glacier surface[8]. The rock material in which the samples are collected makes it much more difficult to visualize individual cells. Microbial diversity in supraglacial environments is higher than microbial diversity under the ice. However, species found in subglacial environments are most often well suited to the subglacial geochemical environment and are often organisms related to other extremophiles[61].

The SEM microscopic studies using an EDS detector allowed the determination of the elemental composition of the tested *A. alaskanum* algae (Fig. 6). The studies showed a homogeneous elemental composition of the tested algal samples. Carbon is the main element constituting over 50% of the mass concentration. Oxygen constitutes over 17% of the mass of *A. alaskanum* algae. The SEM EDS studies showed nitrogen content of over 12% by weight in the tested algae. The *A. alaskanum* algae were compared in terms of the content of elements with

A. nordenskiöldii. Significantly lower oxygen content was found in the *A. alaskanum* cells. Significantly higher contents (12 times) of nitrogen as well as magnesium, sodium, and iron were observed. The silicon concentration was similar in *A. alaskanum* and *A. nordenskiöldii* cells[44].

Using the DIC microscopic and FTIR chemical methods, we analyzed the rock material accompanying algal cells in their natural environment (Figs. 7 and 8). The FTIR spectra showed similarity to nontronite and illite. Nontronite is an iron (III)-rich clay mineral belonging to the common and widespread smectite minerals. It is formed in the process of hydrothermal transformation of silicates. Smectite minerals have specific properties, e.g. susceptibility to water dispersion, ability to exchange cations and sorption of organic substances, and ability to swell and form thixotropic suspensions that do not sediment for a long time[62].

Illite, a mineral from the silicate group, is classified as a clay mineral. It is also a very common and widespread mineral throughout the world. Its particularly large accumulations occur on ocean floors. Nitrogen is held by illite in the form of the NH_4^+ cation, substituting for K + in illite interlayers[63]. This may be related to the increased amount of nitrogen in the cells of the alga *A. alaskanum*, potentially leading to the lower C: N ratio of cca. 56:12 observed in the algal cells. The carbon to nitrogen stochiometry in cryoflora cells was reported to reflect in situ conditions[64]. Assessment of the macro-nutrient stoichiometry of glacier algal assemblages from the southwestern Greenland ice sheet margin reported an elevated C: N ratio of 1.997 to 73 in *Ancylonema* cells[65], which reflects their characteristic oligotrophic environment.

The smectite-to-illite (S-I) reaction is closely related to hydrocarbon maturation, geopressuring of shale, the formation of growth faults, and changes in pore water chemistry[66]. The degree of the S-I reaction is frequently used as a geothomiometer to allow reconstructions of tectonic history of sedimentary basins[67]. Some evidence indicates that microorganisms may play an important role in the formation of silicates[68]. It was demonstrated that microorganisms can promote the S-I reaction by dissolving smectite through reduction of structural Fe(III) in the smectite structure[66]. Iron(III) bound in clay minerals can be an important electron acceptor supporting algal cell growth in natural environments. Whether glacier ice algae are involved in these processes or benefit by enriching their mineral composition is an open question and a problem for further research.

Adaptation of biological and chemical methods for the analysis of algal cells that have not been thoroughly characterized seems to provide valuable knowledge that will allow further comparisons of rare microorganisms living in harsh environmental conditions. Most of the microorganisms living in glacier ice are not yet known. A team of researchers from the Chinese Academy of Sciences examining glaciers on the Tibetan Plateau found a total of 968 species of microorganisms frozen in the ice. Most of them were bacteria, but also algae, archaea, and fungi[69]. The most surprising fact was that approximately 98% of the discovered species were completely unidentified and unknown. This is definitely an unexpected level of biodiversity, considering the challenges of living inside glaciers.

Single-celled microscopic algae living in one of the most extreme habitats on Earth influence the formation of these environments. By reducing albedo, glacier ice algae accelerate the melting of snow caps and glaciers and, therefore, the extent of their blooms can be used to monitor ongoing climate change[17]. Secondary metabolites such as purpurogallin in glacier ice algae protect chloroplasts and nuclei from damage caused by increased ultraviolet (UV) radiation and visible light, while ice-binding proteins and polyunsaturated fatty acids contribute to reducing cell damage associated with exposure to low temperatures and ice-desiccation (on glaciers, liquid water may be only intermittently available due to freezing), characteristic features of glacial environments[17,70]. Purpurogallin is a compound with antioxidant, anticancer, and anti-inflammatory properties. Additionally, its anticancer properties have been proven in esophageal squamous cell carcinoma[71]. This natural compound found in some plants is also an effective hepatoprotector that may act partly or mainly as a xanthine oxidase inhibitor[72]. It has also been proven that purpurogallin was found to have a significant effect on osteoclast differentiation in a dose-dependent manner without causing cytotoxicity[73].

We are particularly interested in the medical properties of glacier ice and snow algae and our future research will aim to expand the knowledge on this subject. We regard these studies as a preliminary stage of these analyses showing us the properties of cells after isolation thereof from their natural environment. The interdisciplinary research has allowed us to better understand and characterize the cells of the glacier ice alga *A. alaskanum*. Its uniqueness and characteristic environment pose new challenges and encourage further exploration of these unique microorganisms.

Data availability

The datasets generated and/or analysed during the current study are not publicly available due to [there was no data requiring statistical analysis during the current study] but original microscopic images and FTIR spectra are available from the corresponding author on reasonable request.

Received: 8 January 2025; Accepted: 24 March 2025
Published online: 27 May 2025

References

1. Möller, M., Recinos, B., Rastner, P. & Marzeion, B. Heterogeneous impacts of ocean thermal forcing on ice discharge from Greenland's peripheral tidewater glaciers over 2000–2021. *Sci. Rep.* **17**, 113–116. https://doi.org/10.1038/s41598-024-61930-6 (2024).
2. Hudson, S. R., Warren, S. G., Brandt, R. E., Grenfell, T. C. & Six, D. Spectral bidirectional reflectance of Antarctic snow: Measurements and parameterization. *J. Geophys. Res. Atmos.* **111**, https://doi.org/10.1029/2006JD007290 (2006).
3. Flanner, M. G., Zender, C. S., Randerson, J. T. & Rasch, P. J. Present-day climate forcing and response from black carbon in snow. *J. Geophys. Res. Atmos.* **112**, https://doi.org/10.1029/2006JD008003 (2007).
4. Flanner, M. G. & Zender, C. S. Linking snowpack microphysics and albedo evolution. *J. Geophys. Res. Atmos.* **111**, https://doi.org/10.1029/2005JD006834 (2006).

5. Healy, S. M. & Khan, A. L. Albedo change from snow algae blooms can contribute substantially to snow melt in the North Cascades, USA. *Commun. Earth Environ.* **4**, 142. https://doi.org/10.1038/s43247-023-00768-8 (2023).
6. Hodson, A. et al. Glacial ecosystems. *Ecol. Monogr.* **78**, 41–67. https://doi.org/10.1890/07-0187.1 (2008).
7. Stibal, M., Šabacká, M. & Žárský, J. Biological processes on glacier and ice sheet surfaces. *Nat. Geosci.* **5**, 771–774. https://doi.org/10.1038/NGEO1611 (2012).
8. Anesio, A. A., Lutz, S., Chrismas, N. A. M. & Benning, L. G. The microbiome of glaciers and ice sheets. *NPJ Biofilms Microbiomes* **3**, https://doi.org/10.1038/s41522-017-0019-0 (2017).
9. Di Mauro, B. et al. Glacier algae foster ice-albedo feedback in the European Alps. *Sci. Rep.* **10**, 4739. https://doi.org/10.1038/s41598-020-61762-0 (2020).
10. Khan, A. L., Dierssen, H. M., Scambos, T. A., Höfer, J. & Cordero, R. R. Spectral characterization, radiative forcing and pigment content of coastal Antarctic snow algae: Approaches to spectrally discriminate red and green communities and their impact on snowmelt. *Cryosphere* **15**, 133–148. https://doi.org/10.5194/tc-15-133-2021 (2021).
11. Cook, J., Edwards, A., Takeuchi, N. & Irvine-Fynn, T. Cryoconite: The dark biological secret of the cryosphere. *Prog. Phys. Geogr.* **40**, 66–111. https://doi.org/10.1177/0309133315616574 (2016).
12. Bøggild, C. E., Brandt, R. E., Brown, K. J. & Warren, S. G. The ablation zone in northeast Greenland: Ice types, albedos and impurities. *J. Glaciol.* **56**, 101–113. https://doi.org/10.3189/002214310791190776 (2010).
13. Di Mauro, B. et al. Impact of impurities and cryoconite on the optical properties of the Morteratsch Glacier (Swiss Alps). *Cryosph.* **11**, 2393–2409. https://doi.org/10.5194/tc-11-2393-2017 (2017).
14. Takeuchi, N. Temporal and spatial variations in spectral reflectance and characteristics of surface dust on Gulkana Glacier. *Alaska Range. J. Glaciol.* **55**, 701–709. https://doi.org/10.3189/002214309789470914 (2009).
15. Remias, D., Procházková, L., Nedbalová, L., Benning, L. G. & Lutz, S. Novel insights in cryptic diversity of snow and glacier ice algae communities combining 18S rRNA gene and ITS2 amplicon sequencing. *FEMS Microbiol. Ecol.* **99**, 134. https://doi.org/10.1093/femsec/fiad134 (2023).
16. Zada, S., Khan, M., Su, Z., Sajjad, W. & Rafiq, M. Cryosphere: A frozen home of microbes and a potential source for drug discovery. *Arch. Microbiol.* **28**, 196. https://doi.org/10.1007/s00203-024-03899-4 (2024).
17. Hoham, R. W. & Remias, D. Snow and glacial algae: A review. *J. Phycol.* **56**, 264–282. https://doi.org/10.1111/jpy.12952 (2020).
18. Barbalace, M. C. et al. Anti-inflammatory activities of marine algae in neurodegenerative diseases. *Int. J. Mol. Sci.* **20**, 3061. https://doi.org/10.3390/ijms20123061 (2019).
19. Procházková, L., Řezanka, T., Nedbalová, L. & Remias, D. Unicellular versus filamentous: The glacial alga *Ancylonema alaskana* comb. et stat. nov. and its ecophysiological relatedness to *Ancylonema nordenskioeldii* (Zygnematophyceae, Streptophyta). *Microorganisms* **9**, 1103 (2021).
20. Remias, D. & Procházková, L. The first cultivation of the glacier ice alga *Ancylonema alaskanum* (Zygnematophyceae, Streptophyta): Differences in morphology and photophysiology of field vs laboratory strain cells. *J. Glaciol.* **69**, 1080–1084. https://doi.org/10.1017/jog.2023.22 (2023).
21. Uetake, J., Naganuma, T., Hebsgaard, M. B., Kanda, H. & Kohshima, S. Communities of algae and cyanobacteria on glaciers in west Greenland. *Polar Sci.* **4**, 71–80. https://doi.org/10.1016/j.polar.2010.03.002 (2010).
22. Onuma, Y. et al. Modeling seasonal growth of phototrophs on bare ice on the Qaanaaq Ice Cap, northwestern Greenland. *J. Glaciol.* **69**, 487–499. https://doi.org/10.1017/jog.2022.76 (2023).
23. Takeuchi, N. & Kohshima, S. A snow algal community on tyndall glacier in the southern Patagonia ice field, Chile. *AAAR* **36**, 92–99 (2004).
24. Ling, H. U. & Seppelt, R. D. Snow algae of the Windmill Islands, continental Antarctica. *Mesotaenium berggrenii* (Zygnematales, Chlorophyta) the alga of grey snow. *Antarct. Sci.* **2**, 143–148. https://doi.org/10.1017/S0954102090000189 (1990).
25. Remias, D., Holzinger, A. & Lütz, C. Physiology, ultrastructure and habitat of the ice alga *Mesotaenium berggrenii* (Zygnematophyceae, Chlorophyta) from glaciers in the European Alps. *Phycologia* **48**, 302–312 (2009).
26. Remias, D., Holzinger, A., Aigner, S. & Lütz, C. Ecophysiology and ultrastructure of *Ancylonema nordenskiöldii* (Zygnematales, Streptophyta), causing brown ice on glaciers in Svalbard (High Arctic). *Polar Biol.* **35**, 899–908. https://doi.org/10.1007/s00300-011-1135-6 (2012).
27. Williamson, C. J. et al. Glacier algae: A dark past and a darker future. *Front. Microbiol.* **10**, 524. https://doi.org/10.3389/fmicb.2019.00524 (2019).
28. Monheit, J. E., Cowan, D. F. & Moore, D. G. Rapid detection of fungi in tissues using calcofluor white and fluorescence microscopy. *Arch. Pathol. Lab. Med.* **108**, 616–618 (1984).
29. Fiołka, M. J. et al. Anti-*Candida albicans* effect of the protein carbohydrate fraction obtained from the coelomic fluid of earthworm *Dendrobaena veneta*. *PLoS ONE* **14**, 0212869. https://doi.org/10.1371/journal.pone.0212869 (2019).
30. Lewtak, K. et al. *Sida hermaphrodita* seeds as a source of anti-*Candida albicans* activity. *Sci. Rep.* **9**, 12233. https://doi.org/10.1038/s41598-019-48712-1 (2019).
31. Meadows, M. G. A batch assay using Calcofluor fluorescence to characterize cell wall regeneration in plant protoplasts. *Anal. Biochem.* **141**, 38–42. https://doi.org/10.1016/0003-2697(84)90422-6 (1984).
32. Herburger, K. & Holzinger, A. Aniline blue and Calcofuor white staining of callose and cellulose in the streptophyte green algae *Zygnema* and *Klebsormidium*. *Bio. Protoc.* **6**, 1969. https://doi.org/10.21769/BioProtoc.1969 (2016).
33. Bidhendi, A. J., Chebli, Y. & Geitmann, A. Fluorescence visualization of cellulose and pectin in the primary plant cell wall. *J. Microsc.* **278**, 164–181. https://doi.org/10.1111/jmi.12895 (2020).
34. Fiołka, M. J. et al. Metabolic, structural, and proteomic changes in *Candida albicans* cells induced by the protein-carbohydrate fraction of *Dendrobaena veneta* coelomic fluid. *Sci. Rep.* **11**, 113205. https://doi.org/10.1038/s41598-021-96093-1 (2021).
35. Wu, S. Q. et al. Covalent labeling of mitochondria with a photostable fluorescent thiol-reactive rhodamine-based probe. *Anal. Methods* **4**, 1699–1703. https://doi.org/10.1039/C2AY25106J (2012).
36. Ludovico, P., Sansonetty, F. & Côrte-Real, M. Assessment of mitochondrial membrane potential in yeast cell populations by flow cytometry. *Microbiology* **147**, 3335–3343. https://doi.org/10.1099/00221287-147-12-3335 (2001).
37. Wójcik-Mieszawska, S., Lewtak, K., Sofińska-Chmiel, W., Wydrych, J. & Fiołka, M. J. Atypical changes in *Candida albicans* cells treated with the Venetin-1 complex from earthworm coelomic fluid. *Sci. Rep.* **13**, 2844. https://doi.org/10.1038/s41598-023-29728-0 (2023).
38. Alemán-Nava, G. S. et al. How to use Nile Red, a selective fluorescent stain for microalgal neutral lipids. *J. Microbiol. Methods* **128**, 74–79. https://doi.org/10.1016/j.mimet.2016.07.011 (2016).
39. Greenspan, P. & Fowler, S. D. Spectrofluorometric studies of the lipid probe. *Nile red. J. Lipid Res.* **26**, 781–789. https://doi.org/10.1016/S0022-2275(20)34307-8 (1985).
40. Cooksey, K. E. et al. Fluorometric-determination of the neutral lipid-content of microalgal cells using Nile red. *J. Microbiol. Methods* **6**, 333–345. https://doi.org/10.1016/0167-7012(87)90019-4 (1987).
41. Fiołka, M. J., Takeuchi, N., Sofińska-Chmiel, W., Mieszawska, S. & Treska, I. Morphological and physicochemical diversity of snow algae from Alaska. *Sci. Rep.* **10**, 19167. https://doi.org/10.1038/s41598-020-76215-x (2020).
42. Thomé, M. P. et al. Ratiometric analysis of acridine orange staining in the study of acidic organelles and autophagy. *J. Cell Sci.* **129**, 4622–4632. https://doi.org/10.1242/jcs.195057 (2016).
43. Cox, C. S. & Wathes, C. M. *Bioaerosols Handbook* 1st edn. (CRC Press, 2020).

44. Fiołka, M. J. et al. Morphological and spectroscopic analysis of snow and glacier algae and their parasitic fungi on different glaciers of Svalbard. *Sci. Rep.* **11**, 21785. https://doi.org/10.1038/s41598-021-01211-8 (2021).
45. Silverstein, R. M., Webster, F. X. & Kiemle, D. J. *Spectrometric identification of organic compounds* 7th edn. (Wiley, 2005).
46. Glassford, S. E., Byrne, B. & Kazarian, S. G. Recent applications of ATR FTIR spectroscopy and imaging to proteins. *Biochim. Biophys. Acta* **1834**, 2849–2858. https://doi.org/10.1016/j.bbapap.2013.07.015 (2013).
47. Kazarian, S. G. & Chan, K. L. A. Applications of ATR-FTIR spectroscopic imaging to biomedical samples. *Biochim. Biophys. Acta* **1758**, 858–867. https://doi.org/10.1016/j.bbamem.2006.02.011 (2006).
48. Berthomieu, C. & Hienerwadel, R. Fourier transform infrared (FTIR) spectroscopy. *Photosynth. Res.* **101**, 157–170. https://doi.org/10.1007/s11120-009-9439-x (2009).
49. Herburger, K. & Holzinger, A. Aniline blue and Calcofluor white staining of callose and cellulose in the ctreptophyte creen Algae *Zygnema* and *Klebsormidium*. *Bio. Protoc.* **6**, 1969. https://doi.org/10.21769/BioProtoc.1969 (2016).
50. Herth, W. & Schnepf, E. The fluorochrome, Calcofluor white, binds oriented to structural polysaccharide fibrils. *Protoplasma* **105**, 129–133. https://doi.org/10.1007/BF01279855 (1980).
51. Herburger, K. & Holzinger, A. Localization and quantification of callose in the streptophyte green algae *Zygnema and Klebsormidium*: correlation with desiccation tolerance. *Plant Cell Physiol.* **56**, 2259–2270. https://doi.org/10.1093/pcp/pcv139 (2015).
52. Permann, C. et al. Induction of conjugation and zygospore cell wall characteristics in the alpine Spirogyra mirabilis (Zygnematophyceae, Charophyta): Advantage under climate change scenarios?. *Plants* **10**, 1740. https://doi.org/10.3390/plants10081740 (2021).
53. Permann, C., Pierangelini, M., Remias, D., Lewis, L. A. & Holzinger, A. Photophysiological investigations of the temperature stress responses of Zygnema spp (Zygnematophyceae) from subpolar and polar habitats (Iceland, Svalbard). *Phycologia* **61**, 299–311. https://doi.org/10.1080/00318884.2022.2043089 (2022).
54. Mazzini, G. & Danova, M. Fluorochromes for DNA staining and quantitation. *Methods Mol. Biol.* **1560**, 239–259. https://doi.org/10.1007/978-1-4939-6788-9_18 (2017).
55. Gottfried, A. & Weinhold, E. Sequence-specific covalent labelling of DNA. *Biochem. Soc. Trans.* **39**, 623–628. https://doi.org/10.1042/BST0390623 (2011).
56. Bucevičius, J., Lukinavičius, G. & Gerasimaitė, R. The use of Hoechst dyes for DNA staining and beyond. *Chemosensors* **6**, 18. https://doi.org/10.3390/chemosensors6020018 (2018).
57. Chazotte, B. Labeling mitochondria with rhodamine 123. *Cold Spring Harb. Protoc.* **7**, 892–894 (2011).
58. Falkowski, P. G. & Raven, J. A. *Aquatic photosynthesis* (Princeton University Press, 2007).
59. Hernández, M. L. & Cejudo, F. J. Chloroplast lipids metabolism and function. A redox perspective. *Front. Plant Sci.* **12**, 712022. https://doi.org/10.3389/fpls.2021.712022 (2021).
60. Moulin, S. L. et al. Fatty acid photodecarboxylase is an ancient photoenzyme that forms hydrocarbons in the thylakoids of algae. *Plant Physiol.* **186**, 1455–1472. https://doi.org/10.1093/plphys/kiab168 (2021).
61. Mikucki, J. & Priscu, J. Bacterial diversity associated with Blood Falls, a subglacial outflow from the Taylor Glacier. *Antarctica. Appl. Environ. Microbiol.* **73**, 4029–4039. https://doi.org/10.1128/AEM.01396-06 (2007).
62. Odom, I. E. Smectite clay minerals: Properties and uses. *Phil. Trans. Roy. Soc. Lond.* **311**, 391–409. https://doi.org/10.1098/rsta.1984.0036 (1984).
63. Środoń, J. Evolution of boron and nitrogen content during illitization of bentonites. *Clay Clay Miner.* **58**, 743–756. https://doi.org/10.1346/CCMN.2010.0580602 (2010).
64. Broadwell, E. L., Pickford, R. E., Perkins, R., Sgouridis, F. & Williamson, C. J. Adaptation versus plastic responses to temperature, light, and nitrate availability in cultured snow algal strains. *FEMS Microbiol. Ecol.* **99**, fiad088. https://doi.org/10.1093/femsec/fiad088 (2023).
65. Williamson, C. J. et al. Macro-nutrient stoichiometry of glacier algae from the southwestern margin of the Greenland Ice Sheet. *Front. Plant Sci.* **12**, 673614. https://doi.org/10.3389/fpls.2021.673614 (2021).
66. Kim, J., Dong, H. L., Seabaugh, J., Newell, S. W. & Eberl, D. D. Role of microbes in the smectite-to-illite reaction. *Science* **303**, 830–832. https://doi.org/10.1126/science.1093245 (2004).
67. Pollastro, R. M. Considerations and applications of the illite/smectite geothermometer in hydrocarbon-bearing rocks of miocene to mississippian Age. *Clay Clay Miner.* **41**, 119–133. https://doi.org/10.1346/CCMN.1993.0410202 (1993).
68. Köhler, B., Singer, A. & Stoffers, P. Biogenic nontronite from marine white smoker chimneys. *Clay Clay Miner.* **42**, 689–701. https://doi.org/10.1346/CCMN.1994 (1994).
69. Liu, Y. et al. A genome and gene catalog of glacier microbiomes. *Nat. Biotechnol.* **40**, 1341–1348. https://doi.org/10.1038/s41587-022-01367-2 (2022).
70. Holzinger, A. & Karsten, U. Desiccation stress and tolerance in green algae: Consequences for ultrastructure, physiological and molecular mechanisms. *Front. Plant Sci.* **4**, 327. https://doi.org/10.3389/fpls.2013.00327 (2013).
71. Xie, X. et al. Purpurogallin is a novel mitogen-activated protein kinase kinase 1/2 inhibitor that suppresses esophageal squamous cell carcinoma growth in vitro and in vivo. *Mol. Carcinog.* **58**, 1248–1259. https://doi.org/10.1002/mc.23007 (2019).
72. Wu, T. W., Zeng, L. H., Wu, J. & Carey, D. Purpurogallin - A natural and effective hepatoprotector *in vitro* and *in vivo*. *Biochem. Cell Biol.* **69**, 747–750. https://doi.org/10.1139/o91-113 (1991).
73. Kim, K. et al. Inhibitory effect of purpurogallin on osteoclast differentiation *in vitro* through the downregulation of c-Fos and NFATc1. *Int. J. Mol. Sci.* **19**, 601. https://doi.org/10.3390/ijms19020601 (2018).

Acknowledgements

This study was supported by the grant project GA24-10019S (Czech Science Foundation) and L.P. has been supported by Charles University Research Centre program (UNCE/24/SCI/006). We thank Daniel Remias (University of Salzburg, Salzburg, Austria) for assistance in the field.

Author contributions

M.J.F. wrote the main manuscript text and preparation of Figs. 2, 9, 10, 4 and 7 and W.S.C. preparation of Figs. 6 and 8, participation in editing the manuscript; L.P. obtaining samples, scientific support, participation in editing the manuscript, preparation of Fig. 1; S.M. preparation of Figs. 3 and 5 and M.D. participation in editing the manuscript; K.S. AFM analysis, visualization of rocks in a confocal microscope; J.W. cell visualization in a confocal microscope. All authors reviewed the manuscript.

Declarations

Competing interests

The authors declare no competing interests.

Additional information

Correspondence and requests for materials should be addressed to M.J.F.

Reprints and permissions information is available at www.nature.com/reprints.

Publisher's note Springer Nature remains neutral with regard to jurisdictional claims in published maps and institutional affiliations.